Mass diffusion of diatomic fluids in random micropore spaces using equilibrium molecular dynamics

Mark Biggs* and Pradeep Agarwal†
Department of Chemical Engineering, University of Adelaide, South Australia 5005, Australia
(Received 10 August 1993)

An equilibrium-molecular-dynamics study of diffusion of a heteronuclear diatomic fluid in random pore systems is reported. The pore space is generated by the use of a simple percolation technique on a tessellation of three-dimensional space with periodic boundary conditions. Simulations using the RATTLE algorithm [H. C. Andersen, J. Comput. Phys. **52**, 24 (1983)] at constant temperature are performed on the percolating cluster only where the substrate atoms are explicitly represented and the substrate-fluid and fluid-fluid interactions are modeled using Lennard-Jones potentials. Using this technique, results are presented for a heteronuclear diatomic molecule (CO-like) within a graphitelike system for porosities between the percolation threshold and $\phi=0.99$, and over the temperature range of $T=100$ K to $T=1500$ K at atmospheric pressure. The results, which include mean-square-displacement and velocity-autocorrelation functions (VACF's), indicate once again that mass diffusion within porous media is fundamentally different from that in the bulk phase. The degree of anomalous behavior tends to decrease with temperature and porosity. Although this is the case, the mean-square-displacement exponent in the long-time limit for the lower porosities ($\phi=0.312$ and $\phi=0.4$) increases with temperature to a limiting value much less than one in the vicinity of $T=300$ K. Trends in the VACF's seen here have been reported in past Lorentz gas simulation studies. Effective diffusion coefficients for our gas-in-pore system were calculated from the VACF's—these appear to vary exponentially with porosity and inverse temperature. This temperature variation is similar to that of a liquid in the bulk phase and hence brings into doubt the use of a temperature-independent tortuosity that relates the diffusion coefficient of a gas in the bulk phase to that within porous media.

PACS number(s): 47.55.Mh, 51.10.+y

I. INTRODUCTION

Recently we reported on an equilibrium-molecular-dynamics (EMD) technique for the study of mass diffusion of atomic fluids within porous media [1]. Results were presented for argon within a completely random graphite porous medium at a temperature of 140 K and fluid density of 3.5 kgm^{-3} for the porosities of 0.312, 0.4, 0.6, and 0.8 and the bulk phase. The results clearly indicated that mass diffusion for such a system was fundamentally different from that in the bulk phase for the simulated conditions. It was shown that the velocity autocorrection functions (VACF's) possessed long negative tails and contained oscillatory components, the mean-square displacements were nonlinear, and the memory kernel of the VACF's decayed slowly. The level of such non-Markovian behavior decreased as the porosity approached 1.

This paper describes the extension of the EMD technique of Ref. [1] to diatomic fluids in particular and molecular fluids in general. The RATTLE algorithm of Andersen [2] was used in conjunction with a Nosé-Hoover (NH) thermostat [3] to study the diffusion of a heteronuclear diatomic molecule (CO-like) within a completely random graphitelike porous medium at atmospheric pressure. Results are presented for porosities of 0.312, 0.4, 0.6, and 0.8 at the temperatures of 100, 200, 300, 500, 700, 1100, 1300, and 1500 K and for porosities of 0.312, 0.4, 0.6, 0.8, 0.95, and 0.99 at a temperature of 900 K. The fluid molecules were represented by a two-center Lennard-Jones potential while the porous solid was the same as in Ref. [1].

II. MOLECULAR-DYNAMICS ALGORITHM

A. Equations of motion

An equilibrium-molecular-dynamics (EMD) simulation in the canonical ensemble (constant *NVT*) for a rigid heteronuclear diatomic fluid (a fluid made up of heteronuclear diatomic molecules with frozen vibrational degrees of freedom) involves the solution for both atoms (1 and 2) of each molecule ($p=1,2,\ldots,P$) the classical trajectory equations modified by Gauss's principle of least constraints [3–5]:

$$\frac{d\mathbf{v}_{1,p}}{dt}=\frac{\mathbf{F}_{1,p}}{m_1}+\mathbf{N}_{1,p}+\mathbf{B}_p,\quad \frac{d\mathbf{r}_{1,p}}{dt}=\mathbf{v}_{1,p}\ , \tag{1a}$$

$$\frac{d\mathbf{v}_{2,p}}{dt}=\frac{\mathbf{F}_{2,p}}{m_2}+\mathbf{N}_{2,p}-\mathbf{B}_p,\quad \frac{d\mathbf{r}_{2,p}}{dt}=\mathbf{v}_{2,p}\ , \tag{1b}$$

where t is time, m the atom mass, and $\mathbf{r}$, $\mathbf{v}$, $\mathbf{F}$, $\mathbf{N}$, and $\mathbf{B}$ are the position, velocity, intermolecular force, Nosé-Hoover (NH) thermostat, and bond constraint vectors, respectively. It should be noted that the bond constraint

*FAX: (618) 303-4373. Electronic address: mib@aelmg.adelaide.edu.au
†Permanent address: Department of Chemical Engineering, University of Wyoming, Laramie, WY 82071.

forces sum to zero for a molecule. The RATTLE algorithm [2] was used to integrate Eqs. (1).

B. Intermolecular force vector

The intermolecular force vector acting on the ith atom is the sum of all potential induced forces that arise from the interaction of that atom with all surrounding atoms except that of the same molecule:

$$\mathbf{F}_i = -\sum_{j=1}^{N_b} \nabla_{r_{ij}} \bar{u}_{ij} \ , \tag{2}$$

where $\bar{u}_{ij}$ is the pair potential function for the atom pair (ij), r_{ij} is the distance between the two atoms, and the gradient operator is defined as

$$\nabla_{r_{ij}} = \frac{d}{dr_{ij}}\hat{\mathbf{r}}_{ijx} + \frac{d}{dr_{ij}}\hat{\mathbf{r}}_{ijy} + \frac{d}{dr_{ij}}\hat{\mathbf{r}}_{ijz} \ . \tag{3}$$

So as to reduce the computational effort associated with force calculation, a modified pair potential function was used—the unmodified pair potential u_{ij} and its gradient were forced to zero at a cutoff radius r_c, determined such that the number of particles within the radius satisfies $N_b \ll N$:

$$\bar{u}_{ij} = \begin{cases} u_{ij} - \left[\dfrac{du_{ij}}{dr_{ij}}\right]_{r_{ij}=r_c} (r_{ij} - r_c) - [u_{ij}]_{r_{ij}=r_c} \\ \qquad\qquad \text{for } r_{ij} < r_c \ , \\ 0 \quad \text{for } r_{ij} \geq r_c \ , \end{cases} \tag{4}$$

where N is the total number of particles within the system. The unmodified pair potentials for the fluid-fluid and fluid-substrate interactions were of the 12-6 Lennard-Jones (LJ) form

$$u_{ij} = 4\varepsilon \left[\left(\frac{\sigma}{r_{ij}}\right)^{12} - \left(\frac{\sigma}{r_{ij}}\right)^{6} \right] , \tag{5}$$

where ε and σ are the pair potential energy and length parameters, respectively.

C. Nosé-Hoover thermostat

The NH thermostat vector for each of the atoms $(i = 1,2)$ of a diatomic molecule are given by [3,4]

$$\mathbf{N}_{i,p} = -\zeta \mathbf{v}_{i,p} \ , \tag{6a}$$

$$\dot{\zeta} = \frac{1}{\tau^2}\left(\frac{2K}{N_{\mathrm{DOF}} k_b T} - 1\right) , \tag{6b}$$

where ζ is the NH Lagrangian multiplier, K the total kinetic energy of the system of molecules, N_{DOF} the total number of degrees of freedom (DOF) in the system, k_b the Boltzmann constant, T the desired temperature and τ the thermostat characteristic time which controls the efficiency of the thermostatting mechanism [3]. The total kinetic energy may be estimated from the atom velocities by

$$K = \tfrac{1}{2}\sum_{i=1}^{N} m_i v_i^2 \ , \tag{7}$$

while the total number of DOF for a system of M rigid diatomic molecules is $2M - 4$.

D. Bond constraint

The bond constraint vector for a molecule is given by [2]

$$\mathbf{B}_p = \lambda_p \mathbf{r}_{12,p} \ , \tag{8}$$

where λ is the bond constraint Lagrangian multiplier and $\mathbf{r}_{12p}$ is the bond length vector

$$\mathbf{r}_{12,p} = \mathbf{r}_{2,p} - \mathbf{r}_{1,p} \ . \tag{9}$$

The bond constraint Lagrangian multiplier is selected for each molecule such that the bond length constraint and its time derivative are satisfied [2]:

$$r_{12,p}^2 - d_{12}^2 = 0 \ , \tag{10a}$$

$$\dot{\mathbf{r}}_{12,p} \cdot \mathbf{r}_{12,p} = 0 \ , \tag{10b}$$

where d_{12} is the desired bond length.

III. SIMULATIONS

A. Conditions and scheme

All simulations involved a heteronuclear diatomic molecule (CO-like: $\sigma_1 = 0.335$ nm, $\varepsilon_1/k_b = 51.2$ K, $m_1 = 1.992\,65 \times 10^{-26}$ kg; $\sigma_2 = 0.295$ nm, $\varepsilon_2/k_b = 61.6$ K, $m_2 = 2.656\,86 \times 10^{-16}$ kg, $d_{12} = 0.1128$ nm where atoms 1 and 2 are C and O, respectively (see p. 21 of Ref. [6]), while the substrate was graphitelike ($\sigma_s = 0.384$ nm and $\epsilon_s/k_b = 58.3$ K) with a stacking spacing of 0.3354 nm and of hexagonal form [7]. The potential parameters for interaction between unlike atoms were determined using the Lorentz-Berthelot rules (see p. 21 of Ref. [6]) for $i \neq j = 1$, 2, and s,

$$\sigma_{ij} = \tfrac{1}{2}(\sigma_i + \sigma_j) \ , \tag{11a}$$

$$\varepsilon_{ij} = (\varepsilon_i \varepsilon_j)^{1/2} \ . \tag{11b}$$

The pore system was generated by the method described in [1] where the unit cells were once again 1.2762 by 0.9839 by 1.3436 nm^3 in size. It should be noted that because the unit cells are of one size, the present method of pore system generation results in the average pore size increasing with porosity. This in effect means the diffusion process will develop from Knudsen-like (where fluid-substrate interactions will dominate) to ordinarylike (where fluid-fluid interactions will dominate) as the porosity increases. Future developments aim to remove this restriction so as to give control over the diffusion regime to be simulated and allow the investigation of porosity and pore size effects independently.

All simulations reported here were performed in reduced units based upon the average of the fluid atom parameters (see Appendix B of Ref. [6]). Examples of reduced quantities include temperature $T^* = Tk_b/\varepsilon$, time

$t^*=t\sigma\sqrt{m/\varepsilon}$, and distance $r^*=r/\sigma$. The cutoff radius for both fluid-fluid and fluid-substrate interactions was 2.5 in reduced units.

Two realizations were done for each of the porosities 0.312, 0.4, 0.6, and 0.8 at each of the temperatures, 100, 200, 300, 500, 700, 900, 1100, 1300, and 1500 K while further simulations were carried out at the porosities of 0.95 and 0.99 for 900 K. The limited number of realizations and the approximate nature of the potential parameters mean that only a qualitative discussion of the results will be possible.

The following procedure was repeated for each simulation:

(a) Following Ref. [1], a completely random pore space was generated with the desired porosity.

(b) The fluid molecules (number of molecules varied from 30 to 100) were distributed randomly throughout the percolating pore space. The geometric center of each molecule was placed in the center of the allocated void unit cell to avoid large initial forces which could cause problems with the time integration scheme.

(c) Each atom was assigned a velocity such that the square of its magnitude was distributed uniformly around the value which would give the desired ensemble temperature. The direction of the velocity vector and the orientation of the molecules were randomly generated under the constraint (10b).

(d) The trajectories were first advanced approximately 30 000 times steps to ensure that equilibrium had been reached. This was followed by the production run during which the mean-square-displacement and velocity-autocorrelation functions were accumulated. The time step used for all simulations was 0.005 ps and production runs were 370 000 times steps long.

B. Results generated

The results generated during each simulation included the mean-square displacement of the molecular center of mass

$$R^2(t)=\langle[\mathbf{r}(t_0+\tau_A)-\mathbf{r}(t_0)]^2\rangle \ , \tag{12}$$

and the velocity-autocorrelation function (VACF) of the molecular center of mass

$$\psi(t)=\langle\mathbf{v}(t_0+\tau_B)\cdot\mathbf{v}(t_0)\rangle \ . \tag{13}$$

The equilibrium ensemble averages, which were averaged over $M\approx 20\,000$ time steps for each simulation, are (see p. 185 of Ref. [6]):

$$\langle[\mathbf{r}(t_0+\tau_A)-\mathbf{r}(t_0)]^2\rangle = \frac{1}{MP}\sum_{j=1}^{M}\sum_{p=1}^{P}[\mathbf{r}_p(t_{0j}+\tau_A)-\mathbf{r}_p(t_{0j})]^2 \ , \tag{14}$$

$$\langle\mathbf{v}(t_0+\tau_B)\cdot\mathbf{v}(t_0)\rangle=\frac{1}{MP}\sum_{j=1}^{M}\sum_{p=1}^{P}\mathbf{v}_p(t_{0j}+\tau_B)\cdot\mathbf{v}_p(t_{0j}) \ , \tag{15}$$

where t_{0j} $(j=1,\ldots,M)$ represents the jth time origin and τ_A (set equal to 100 time steps) and τ_B (set equal to 10 time steps) are the time steps between successive quantities used in the calculation of the mean-square-displacement and velocity-autocorrelation functions, respectively. The diffusion coefficient D, was estimated using (see p. 60 of Ref. [6]),

$$D\approx\tfrac{1}{3}\int_0^{t_u}\psi(t)dt \ , \tag{16}$$

where t_u is the length of the generated VACF. The diffusion coefficients may be overestimated to some degree by this equation at $\phi=0.312$ and $\phi=0.4$ due to long negative tails.

IV. RESULTS AND DISCUSSION

A. Mean-square displacement function

The motion of a particle with velocity $\mathbf{v}$ and mass m within a system of interacting particles may be modeled by the non-Markovian Langevin equation (see p. 31 of Ref. [8])

$$\frac{d\mathbf{v}}{dt}=-\int_{-\infty}^{t}\gamma(t-t')\mathbf{v}(t')dt=\frac{1}{m}\mathbf{R}(t) \ , \tag{17}$$

where the integral term represents the non-Markovian friction forces on the particle due to its motion relative to the rest of the fluid and $\mathbf{R}(t)$ is a random force that arises from the particle's interaction with it surroundings. If the friction kernel $\gamma(t-t')$ is assumed to scale as

$$\gamma(t-t')\sim\delta(t-t') \ , \tag{18}$$

where $\delta(t-t')$ is the Dirac δ function, then Eq. (17) may be simplified to the linear Langevin equation

$$\frac{d\mathbf{v}}{dt}=-\gamma\mathbf{v}(t)+\frac{1}{m}\mathbf{R}(t) \ . \tag{19}$$

If we assume that the random force is short lived and its average is zero, then the mean-square-displacement function scales as (see p. 455 of Ref. [9])

$$R^2(t)\sim\begin{cases}t^2 & \text{for } t\to 0, \quad (20a)\\ t & \text{for } t\to\infty \ , \quad (20b)\end{cases}$$

where the short- and long-time limiting behaviors may be classified as Newtonian dynamics and normal diffusion, respectively. Transition between the two regimes is caused by particle-particle interactions. It has been shown that for anomalous diffusion, the mean-square displacement scales as [10,11]

$$R^2(t)\sim t^{\alpha} \ , \tag{21}$$

where α is less than 1 in the long-time limit.

The variation of α at small times with temperature for different porosities is illustrated in Fig. 1(a)—the values of α were derived from the straight-line fit of the log-log plots of the mean-square-displacement function at small times and the confidence bands account for errors associated with the fitting process only. Figure 1(a) indicates that in the short-time limit, the α exponent increases with temperature towards a limiting value of $\alpha\approx 1.65$ and 1.4

for $\phi=0.8$ and 0.6, respectively, while it increases to a peak at $T\approx 500$ K for $\phi=0.4$ ($\alpha\approx 1.23$) and $\phi=0.6$ ($\alpha\approx 1.18$). It is clear that the assumptions used in developing the limiting behavior (20a) may not be valid for particle motion within our porous medium. The short-time behavior seen here does not correspond with that reported by El Amrani and Kolb [12], who do get the limiting behavior of (20a)—this difference may be due to pore size effects.

The variation of α at large times with temperature for different porosities is illustrated by the solid lines in Fig. 1(b)—the values of α were derived from the straight-line fit of the log-log plots of the mean-square-displacement function in the neighborhood of $t^*\approx 80$. Figure 1(b) indicates that α in the long-time limit increases towards unity with porosity for temperatures $T\geq 200$ K and with temperature for $\phi=0.6$ and 0.8. Further, the α exponent increases with temperature to the limiting values of $\alpha\approx 0.6$ for $\phi=0.312$ and $\alpha\approx 0.75$ for $\phi=0.4$. These limiting values are greater than that for a random walker on the sample spanning cluster at the percolation threshold [10] [shown as dashed line $\alpha\approx 0.57$ in Fig. 1(b)]. Some sense of these behaviors may be made if we consider the fundamental basis of anomalous diffusion. The correlation length of a percolation system is the distance a particle must move from its origin before it "forgets" its initial state—this distance dictates the length of memory of a diffusion process. Near the percolation threshold ϕ_c, the correlation length of a percolation system of porosity ϕ scales according to

$$\xi\sim|\phi-\phi_c|^{-\nu}, \tag{22}$$

where ν is a positive universal scaling exponent [13]. From Eq. (22) it may be seen that, for a given temperature, memory (i.e., time taken for a particle to "forget" its initial state) increases as the porosity decreases towards the percolation threshold and, for a given porosity, memory decreases as the temperature increases (because as temperature increases, a particle will take less time on average to exceed the correlation length). This would account for the increase of α at large times with temperature for $\phi=0.6$ and 0.8 and with porosity for $T\geq 200$ K. The behavior of α in the long-time limit at $\phi=0.312$ and 0.4 shall be discussed below.

The transition from short- to long-time behavior for the different porosities at $T=500$ K is clearly shown in Fig. 1(c)—this plot will display horizontal straight-line behavior corresponding to α when the mean-square displacement is governed by Eq. (21). Based upon the above discussion, one would expect, for $\phi>\phi_c$, the α exponent to change from $1<\alpha<2$ at short times to $\alpha<1$ (anomalous diffusion) at intermediate times and finally to $\alpha=1$ (normal diffusion) at long times. It appears as if this sequence of transitions does occur for $\phi=0.6$ in the time span shown where the process passes from anomalous diffusion in the range $10\lesssim t^*\lesssim 20$ to normal diffusion for $t^*\gtrsim 50$. The short-to-intermediate-time behavior for $\phi=0.312$ and 0.4 are similar to that of $\phi=0.6$. However, the point of transition from anomalous to normal diffusion for these lower porosities is much greater than that for $\phi=0.6$—the transition does not occur in the time span shown here. This type of behavior is not dissimilar to that reported by Lowe and Masters [14] for a Lorentz system where they found that the time of onset of asymptotic behavior shifted rapidly to longer times as the percolation threshold was approached. The process for $\phi=0.8$ is very different from that of the other porosities where it makes a transition directly from $\alpha>1$ at short times to normal diffusion at long times without passing through an anomalous-diffusion regime. The above transition behaviors are seen at all temperatures $T\geq 200$ K where the time taken to reach the Gaussian limit at $\phi=0.8$ decreases with increasing temperature and the period of anomalous diffusion at $\phi=0.6$ becomes smaller with increasing temperature. The behavior of the α exponent for all porosities at $T=100$ K may be caused by the nearness of $T=100$ K to the gas-liquid transition temperature for carbon monoxide (allowing for the fact that our fluid is only CO-like)—the mean-square-displacement function shown in Fig. 2(a) for $T=100$ K indicates a highly immobile fluid relative to that at $T=200$ K shown in Fig. 2(b).

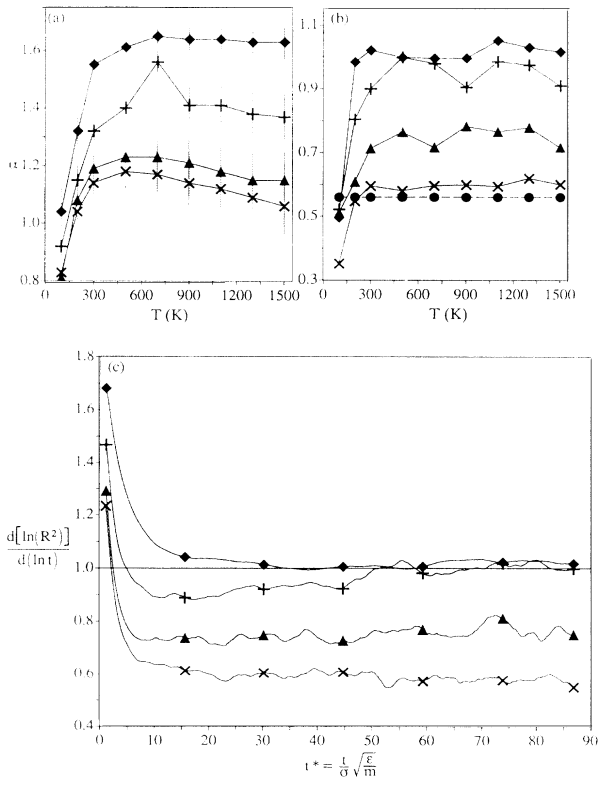

FIG. 1. (a) Variation of α at small times with temperature (95% confidence bands shown). ×, $\phi=0.312$; ▲, $\phi=0.4$; +, $\phi=0.6$; ♦, $\phi=0.8$. (b) Variation of α at large times with temperature. ×, $\phi=0.312$; ▲, $\phi=0.4$; +, $\phi=0.6$; ♦, $\phi=0.8$; ●, $\phi=\phi_c$ [10]. (c). Derivative of log-mean-square-displacement with respect to log time vs reduced time. ×, $\phi=0.312$, ▲, $\phi=0.4$; +, $\phi=0.6$; ♦, $\phi=0.8$.

B. Velocity-autocorrelation function

The velocity-autocorrelation functions for all porosities are plotted for $T\leq 300$ K and 900 K in Figs. 3(a)–3(d).

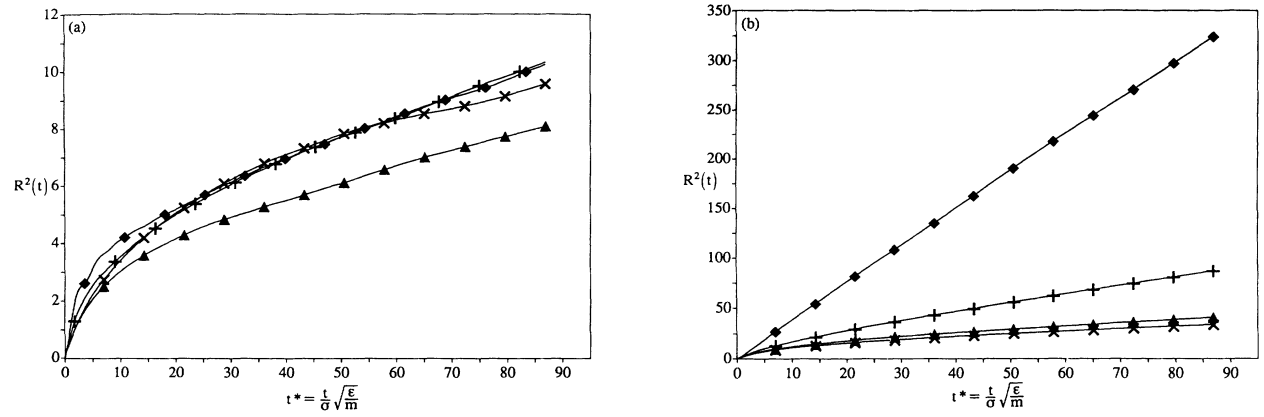

FIG. 2. (a) Reduced mean-square-displacement function for $T=100$ K. ×, $\phi=0.312$; ▲, $\phi=0.4$; +, $\phi=0.6$; ♦, $\phi=0.8$. (b) Reduced mean-square-displacement function for $T=200$ K. ×, $\phi=0.312$; ▲, $\phi=0.4$; +, $\phi=0.6$; ♦, $\phi=0.8$.

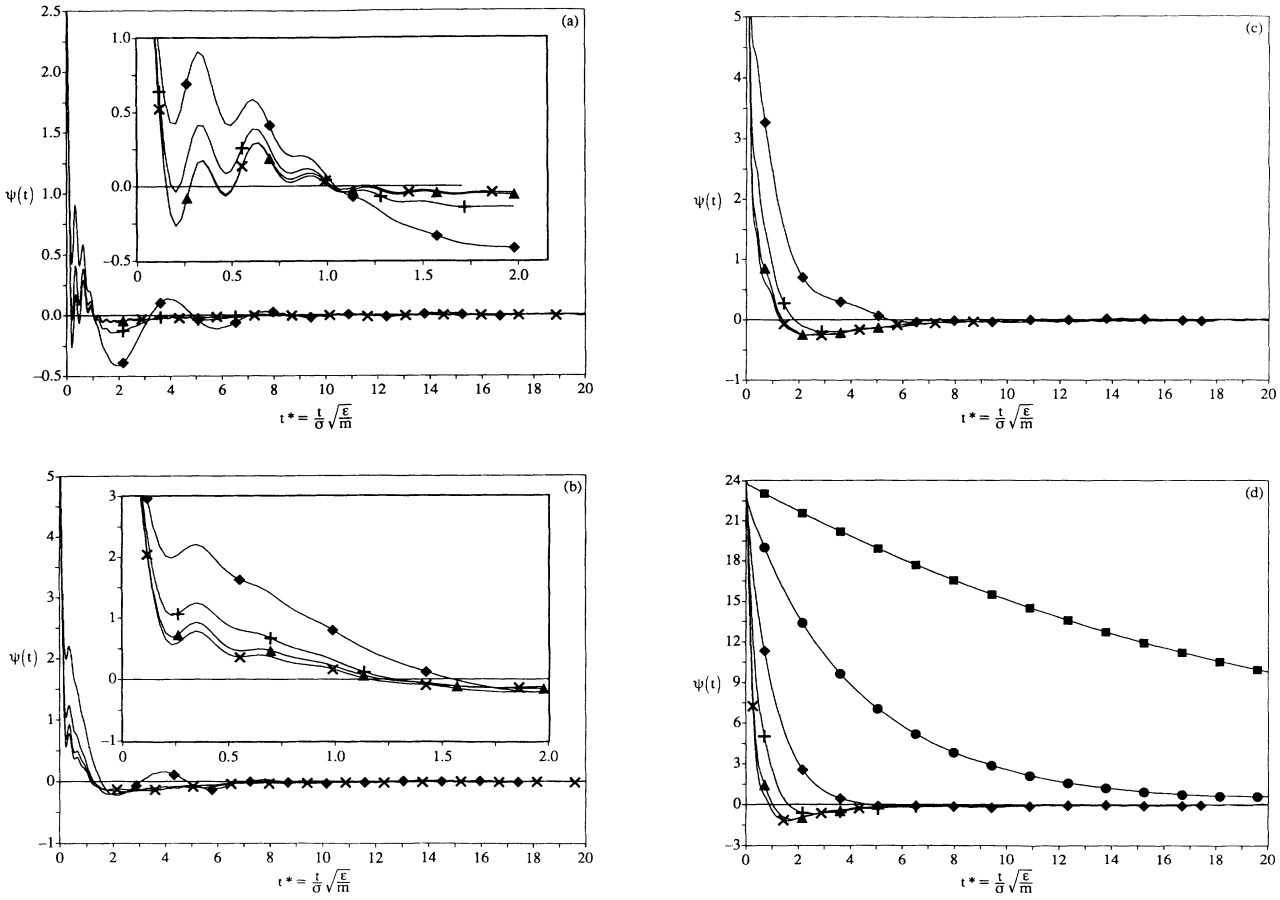

FIG. 3. (a) Reduced velocity-autocorrelation function vs reduced time for $T=100$ K. ×, $\phi=0.312$; ▲, $\phi=0.4$; +, $\phi=0.6$; ♦, $\phi=0.8$. (b) Reduced velocity-autocorrelation function vs reduced time for $T=200$ K. ×, $\phi=0.312$; ▲, $\phi=0.4$; +, $\phi=0.6$; ♦, $\phi=0.8$. (c) Reduced velocity-autocorrelation function vs reduced time for $T=300$ K. ×, $\phi=0.312$; ▲, $\phi=0.4$; +, $\phi=0.6$; ♦, $\phi=0.8$. (d) Reduced velocity-autocorrelation function vs reduced time for $T=900$ K. ×, $\phi=0.312$; ▲, $\phi=0.4$; +, $\phi=0.6$; ♦, $\phi=0.8$; ●, $\phi=0.95$; ■, $\phi=0.99$.

The VACF's for $T \leq 200$ K display strong oscillatory behavior—the source of these oscillations is discussed in Biggs and Agarwal [1]. For $T \geq 300$ K and $\phi \leq 0.6$, the VACF's display long negative tails. Both the oscillatory and long-time tail behaviors have been seen in Lorentz gas simulation studies [15,16]. The VACF's for $T \geq 300$ K and $\phi \geq 0.8$ display gaslike behaviors while liquidlike characteristics may be seen at all other porosities and temperatures $T \geq 200$ K.

C. Effective diffusion coefficient

The log of the reduced effective diffusion coefficient is illustrated for each temperature against porosity ($0.312 \leq \phi \leq 0.8$) in Fig. 4(a). This plot indicates that the effective diffusion coefficient at a given temperature ($T \geq 200$ K) for $0.312 \leq \phi \leq 0.8$ varies as

$$D_e = k_1 e^{\beta\phi} , \tag{23}$$

where the variations of β and k_1 with temperature are shown in Figs. 4(b) and 4(c), respectively. The preexponential factor appears to be a weak function of temperature, while it is unclear if β varies with temperature at all due to the large error bands; these errors could be reduced if more results at different porosities were generated so as to increase the number of degrees of freedom used in generating confidence intervals.

The log of the reduced effective diffusion coefficient is shown for each porosity against inverse temperature in Fig. 5(a). This plot indicates that the effective diffusion coefficient at a given porosity ($0.312 \leq \phi \leq 0.8$) for $T \geq 200$ K varies as

$$D_e = k_2 e^{\lambda/T} , \tag{24}$$

where the variations of λ and $\ln(k_2)$ with porosity are shown in Figs. 5(b) and 5(c), respectively. The preexponential factor appears to vary exponentially with porosity and thus verifies the form of Eq. (23). The exponential factor λ appears to decrease as the porosity increases from $\phi = 0.312$ to 0.6. However, it is unclear if λ reaches a plateau or increases with porosity for $\phi > 0.6$.

This variation of the effective diffusion coefficient with temperature is similar to that of liquids in the bulk phase (see p. 587 of Ref. [17]) and is in marked contrast to the $T^{3/2}$–T^2 variation predicted from kinetic theory for gases in the bulk phase (see p. 564 of Ref [17]). This brings into doubt the validity of the much used

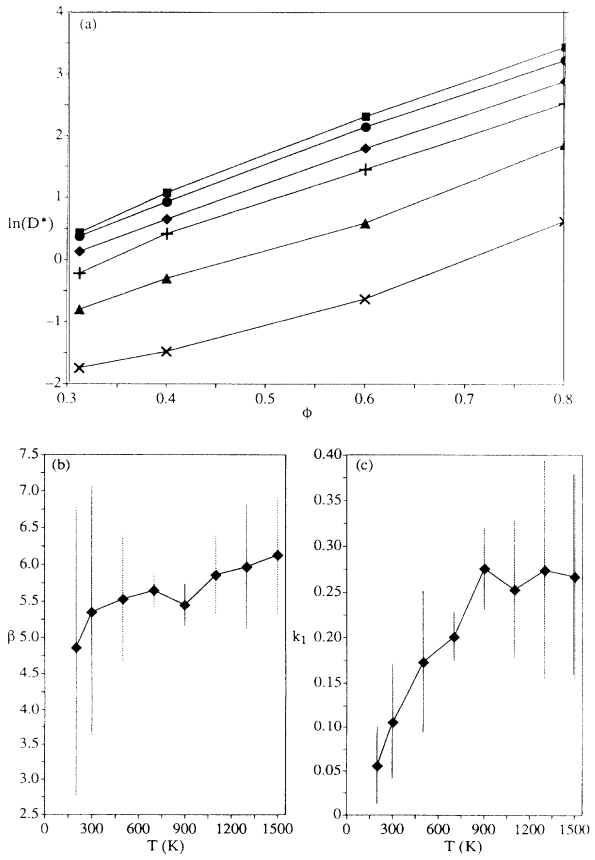

FIG. 4. (a) Log of reduced effective diffusion coefficient vs porosity for each temperature. ×, $T=200$ K; ▲, $T=300$ K; +, $T=500$ K; ♦, $T=700$ K; ●, $T=1100$ K; ■, $T=1500$ K. (b) Variation of the β exponent with temperature (95% confidence bands shown). (c) Variation of the k_1 factor with temperature (95% confidence bands shown).

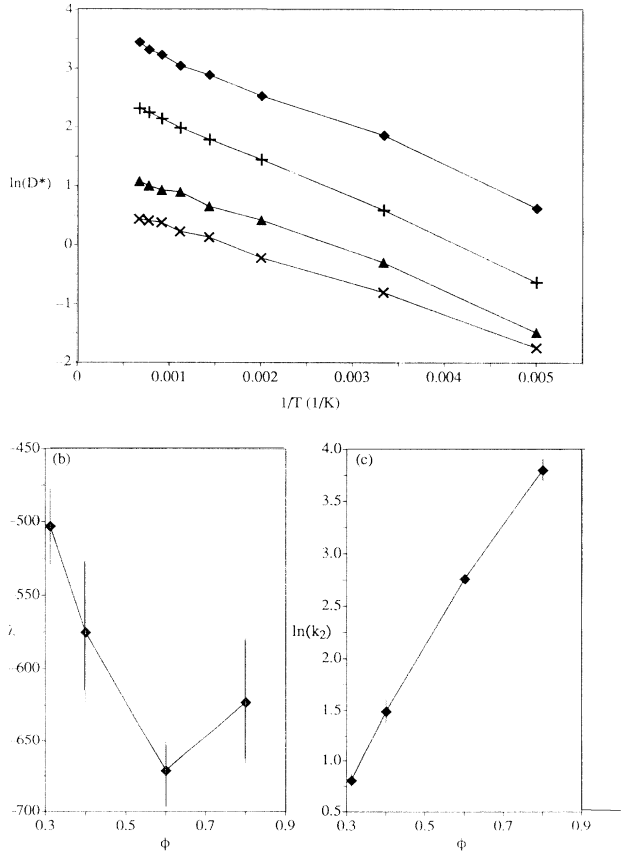

FIG. 5. (a) Log of the reduced effective diffusion coefficient vs inverse temperature. ×, $\phi=0.312$; ▲, $\phi=0.4$; +, $\phi=0.6$; ♦, $\phi=0.8$. (b) Variation of λ exponent with porosity (95% confidence bands shown). ×, $\phi=0.312$; ▲, $\phi=0.4$; +, $\phi=0.6$; ♦, $\phi=0.8$. (c) Variation of the k_2 factor with porosity (95% confidence bands shown). ×, $\phi=0.312$; ▲, $\phi=0.4$; +, $\phi=0.6$; ♦, $\phi=0.8$.

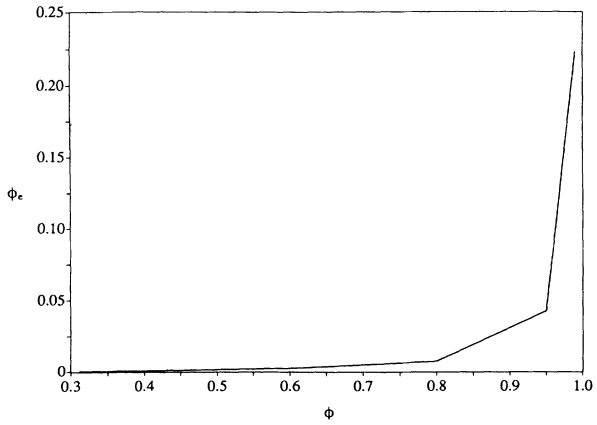

FIG. 6. Normalized effective diffusion coefficient vs porosity for $T=900$ K.

temperature-independent tortuosity (see, for example, Ref. [18]) that relates the diffusion coefficient of a gas in the bulk phase to that within a porous media. This result is supported by the work of Bhatia [19], who demonstrated that the tortuosity may be dependent upon temperature, pressure, and the diffusing gases.

The variation of the normalized effective diffusion coefficient, $\phi_e = D_e/D$, where D is assumed to be the diffusion coefficient for CO in the bulk phase, with porosity ($0.312 \leq \phi \leq 0.99$) for $T=900$ K is shown in Fig. 6. Allowing for the fact that the fluid used in the simulations was only CO-like, Fig. 6 shows that even at $\phi=0.99$, the calculated effective diffusion coefficient is still five times smaller than that in the bulk phase. Similar behavior has been reported in Reyes and Jensen [20].

V. SUMMARY AND CONCLUSIONS

The results, once again, indicate that there are clear differences between mass diffusion within porous media and mass diffusion in the bulk phase. In the short-time limit, the mean-square-displacement exponent is less than 2 but greater than 1 for all conditions simulated except at $T=100$ K, while in the long-time limit, the exponent is less than 1 for low porosities at all temperatures and for all porosities up to $T=300$ K. In all cases except $T=100$ K, the mean-square-displacement exponent in the long-time limit exceeded that of a random walker on the sample spanning cluster at the percolation threshold—the behavior at $T=100$ K could be caused by the nearness of this temperature to the gas-liquid transition point of the fluid simulated. The VACF's display oscillatory components and long negative tails at the lower temperatures and long negative tails at all temperatures for the lower porosities. The qualitative behaviors seen here are similar to those reported in Lorentz gas simulation studies [14–16].

The effective diffusion coefficient appears to vary exponentially with porosity and inverse temperature. The temperature variation is similar to that of liquid in the bulk phase and corresponds to the liquidlike behavior seen in the VACF's. The liquid-type variation with temperature means that the use of a temperature-independent tortuosity factor that relates the diffusion coefficient of a gas in the bulk phase to that within a porous media may be insufficient.

The present method of pore system generation means that the average pore size increases with porosity. This is undesirable and hence the method detailed here is presently being extended to allow independent control over both pore size and porosity. Future papers will address this issue and the effects of fluid-substrate energy exchange and reaction.

ACKNOWLEDGMENTS

The calculations upon which this work is based were carried out using the Fujitsu VP2200 supercomputer of the Australian National University Supercomputing Facility (ANUSF). One of the authors (M.J.B.) would like to thank Dr. Roger Edburg and Dr. Bob Gringold of the ANUSF for many helpful discussions and the University of Adelaide for support.

[1] M. Biggs and P. Agarwal, Phys. Rev. A **46**, 3312 (1992).
[2] H. C. Andersen, J. Comput. Phys. **52**, 24 (1983).
[3] D. J. Evans and B. L. Holian, J. Chem. Phys. **83**, 4069 (1985).
[4] C. Pierleoni and J. P. Ryckaert, Mol. Phys. **75**, 731 (1992).
[5] T. C. Bradbury, *Theoretical Mechanics* (Wiley, New York, 1968), Chap. XI.
[6] M. P. Allen and D. J. Tildeseley, *Computer Simulations of Liquids* (Oxford University, New York, 1989).
[7] *Concise Encyclopedia of Chemical Technology,* edited by M. Grayson and D. Eckroth (Wiley, New York, 1985), Vol. 4, p. 305.
[8] R. Kubo, M. Toda, and N. Hashitsume, *Statistical Physics II: Nonequilibrium Statistical Mechanics* (Springer-Verlag, Berlin, 1985).
[9] D. A. McQuarrie, *Statistical Mechanics* (Harper and Row, New York, 1976).
[10] Y. Gefen, A. Aharony, and S. Alexander, Phys. Rev. Lett. **50**, 77 (1983).
[11] R. Muralidhar, D. Ramkrishna, H. Nakanishi, and D. Jacobs, Physica A **167**, 539 (1990).
[12] S. El Amrani and M. Kolb, J. Chem. Phys. **98**, 1509 (1993).
[13] M. Sahimi, G. G. Gavalas, and T. T. Tsotsis, Chem. Eng. Sci. **45**, 1443 (1990).
[14] C. P. Lowe and A. J. Masters, Physica A **195**, 149 (1993).
[15] C. Bruin, Physica **72**, 261 (1974).
[16] C. P. James and G. T. Evans, J. Chem. Phys. **87**, 4056 (1987).
[17] R. C. Reid, J. M. Prausnitz, and T. K. Sherwood, *The Properties of Gases and Liquids,* 3rd ed. (McGraw-Hill, New York, 1977).
[18] N. Epstein, Chem. Eng. Sci. **44**, 777 (1989).
[19] S. K. Bhatia, Chem. Eng. Sci. **41**, 1311 (1986).
[20] S. Reyes and K. F. Jensen, Chem. Eng. Sci. **40**, 1723 (1985).